JGR Solid Earth

RESEARCH ARTICLE
10.1029/2024JB029236

Tectonic Quiescence in Actively Extending Back-Arc Regions

A. Beniest[1,2], A. Dannowski[1], M. Schnabel[3], H. Kopp[1], and the SO267 Scientist Party[4]

[1]GEOMAR, Helmholtz Centre for Ocean Research Kiel, Kiel, Germany, [2]Department of Earth Sciences, Vrije Universiteit Amsterdam, Amsterdam, The Netherlands, [3]BGR, Federal Institute for Geosciences and Natural Resources, Hannover, Germany, [4]See Appendix A

Key Points:

- The crustal structure of the central Lau Basin at 18°S complies with typical back-arc/arc crustal velocities and thickness
- South of the FRSC no plate boundary is observed, suggesting one Niuafo'ou-Tonga plate with zones of intraplate deformation
- High crustal P-wave velocities result from the crystalisation of hydrous melts (upper crust) and pyroxene-rich material (lower crust)

Correspondence to:

A. Beniest,
a.beniest@vu.nl

Citation:

Beniest, A., Dannowski, A., Schnabel, M., Kopp, H., & the SO267 Scientist Party (2024). Tectonic quiescence in actively extending back-arc regions. *Journal of Geophysical Research: Solid Earth*, *129*, e2024JB029236. https://doi.org/10.1029/2024JB029236

Received 3 APR 2024
Accepted 3 SEP 2024

Author Contributions:

Conceptualization: A. Beniest, A. Dannowski, H. Kopp
Data curation: A. Dannowski, M. Schnabel
Formal analysis: A. Beniest, A. Dannowski, M. Schnabel
Funding acquisition: A. Beniest, H. Kopp
Investigation: A. Beniest, A. Dannowski, M. Schnabel
Methodology: A. Beniest, A. Dannowski, M. Schnabel
Project administration: H. Kopp
Resources: A. Beniest, A. Dannowski
Software: M. Schnabel
Supervision: A. Dannowski, M. Schnabel, H. Kopp
Validation: A. Beniest, A. Dannowski, M. Schnabel
Visualization: A. Beniest, A. Dannowski, M. Schnabel
Writing – original draft: A. Beniest, A. Dannowski

Abstract

We analyzed refraction and reflection seismic data covering the Central Lau Spreading Center (CLSC) and the Tonga volcanic arc at 18°S in the Pacific Ocean to investigate tectonic inactivity in actively extending back-arc systems. Our P-wave travel time tomography shows a characteristic 6–8 km thick back-arc crust beneath and around the CLSC and a ∼13 km thick arc-crust at the eastern end of our profile, which corresponds to the Tonga volcanic arc. Lower crustal velocities increase to 7.5 km/s toward the volcanic arc, marking the transition from back-arc to arc crust. These high P-wave velocities can be explained by a high pyroxene content in the lower crust originating from depleted melts. Our seismic reflection data show steep normal faults below the CLSC and volcanic structures closer to the volcanic arc, without a tectonically inactive zone (also knows as the "diffuse plate boundary") in between. Based on our results, we suggest that the Niuafo'ou and Tonga microplates should be treated as one tectonic plate with local zones of intra-plate deformation that are separated by zones that are tectonically quiet.

Plain Language Summary

In a subduction zone one tectonic plate sinks below another. A retreating downgoing plate causes tension in the overriding plate, which leads to thinning behind the volcanic arc: a back-arc basin is born. We investigate the crustal structure of a seismically inactive region within a back-arc basin in overall extension. Our aim is to understand why there is no seismic activity in this specific area. The Lau Basin is our case study, because it is a type-example for back-arc basin tectonics. We have acquired and interpreted seismic data to analyse the structure of the crust along a profile in the Lau Basin. We observe crustal thickness changes from typical back-arc crust (6 and 7 km) to arc-crust (13 km), and volcanic remnants in the crust with higher crustal velocities. Current tectonic activity only occurs at the Central Lau Spreading Center (CLSC), not in between the CLSC and the volcanic arc. We therefore reject the idea of a diffuse plate boundary, and propose that the Niuafo'ou and Tonga microplates should be treated as one tectonic plate that consists of localized zones that deform. In between those actively extending zones, there are areas that do not deform and that are tectonically quiet.

1. Introduction

Extension accommodation in back-arc regions is highly variable and non-linear, meaning that the location of extension relocates over time often multiple times, and differs per back-arc system. In the Scotia Sea region for example, subduction and subsequent extension initiated at the transition between oceanic and continental crust (Schellart et al., 2023), but since 32 Ma extension is accommodated along sharply defined, active spreading centers (Eagles et al., 2005). In the Aegean Sea, extension is accommodated in a more distributed way since the Eocene (Beniest et al., 2016; Brun et al., 2016), extending predominantly continental crust (Makris et al., 2022; Tirel et al., 2004). This multifaceted evolution of back-arc basins is the result of a combination between subduction-extension interaction (Sdrolias & Müller, 2006), nature of the overriding plate (e.g., oceanic vs. continental; Artemieva, 2023), the internal crustal structure of the overriding plate (Grevemeyer et al., 2021) and the morphological heritage of the upper plate (Palmiotto et al., 2022).

Back-arc basin tectonics were first described in the Tonga-Kermadec subduction and its accompanying back-arc system in the southwest Pacific Ocean (Karig, 1970). This subduction system has a convergence rate of maximum 240 mm/yr (Bevis et al., 1995) above which the Tonga volcanic arc developed. The Tonga volcanic arc is a type-example for intra-oceanic subduction volcanism (Smith & Price, 2006). The Lau Basin is a back-arc basin that formed behind the Tonga volcanic arc. In the Lau Basin, extension is accommodated in the oceanic crust that formed along several segments of back-arc spreading that delineate the overriding plate (Anderson et al., 2021).

Writing – review & editing: A. Beniest, A. Dannowski, M. Schnabel, H. Kopp

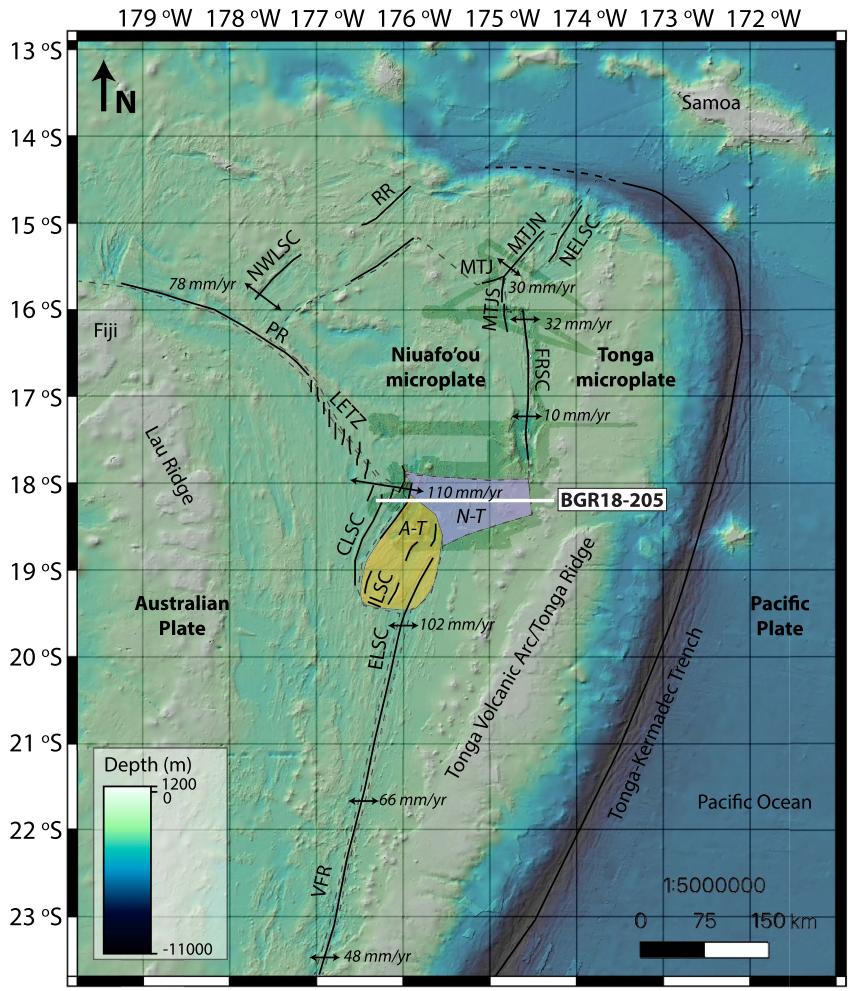

Figure 1. Bathymetric map of the Lau Basin with profile BGR18-205 indicated in white. The Lau Basin hosts the Niuafo'ou and Tongan microplates and is bordered by the Australian and Pacific plates. A-T represents the diffuse plate boundary between the Australia plate and Niuafo'ou and Tonga microplates. N-T represents the not well-established diffuse plate boundary. Plate velocities, plate boundaries and active deformation zones are adopted from Sleeper and Martinez (2016).

This extension initially occurred along the complete extent of the plate boundary (Ruellan et al., 2003), but rifting and spreading became more localized after ~4 Ma. This localization lead to the formation of multiple micro-crustal blocks (Chase, 1971) and an amalgamation of rifts, spreading centers and ridges, with highly varying extension rates between 10–110 mm/yr (Baxter et al., 2020) (Figure 1). These are, from north going anti-clockwise (Figure 1), the Rochambeau Rift (RR), North-West Lau Spreading Center (NWLSC), the Futuna Spreading Center (FSC), the Peggy Ridge (PR), the Lau Extensional Transform Zone (LETZ), the Central Lau Spreading Center (CLSC), the Intermediate Lau Spreading Center (ILSC), the Eastern Lau Spreading Center (ELSC), the Valu Fa Ridge (VFR), the Fonualei Rift and Spreading Center (FRSC), the Mangatolu Triple Junction (MTJ), the North-East Lau Spreading Center (NELSC).

Numerical models have shown that active deformation in the mantle below the back-arc domain is possible over wide distances, in this case from near the Tonga trench until 800 km away below the overriding plate (Palmiotto et al., 2022). In between these rift and spreading centers, there are seismically inactive regions. These regions have not recorded large (Mw > 5), shallow (<30 km) seismic events (Baxter et al., 2020; Conder & Wiens, 2011) since recording started, and appear not to be affected by the tension exerted on the overriding plate by the retreating subducting slab for longer periods of time. This occurs for example, in between the CLSC and the Tonga volcanic arc (purple shaded area, Figure 1), where there is a lack of shallow (<10 km deep) seismicity (Baxter et al., 2020), hinting to tectonic quiescence.

Despite seismic inactivity, kinematic models use such areas to accommodate extension in a diffuse or distributed way. In the northern Lau Basin this was done by acknowledging the Niuafo'ou micro-crustal block (Zellmer & Taylor, 2001) that is surrounded by spreading centers with varying opening rates in combination with the implementation of a diffuse plate boundary zone in between the CLSC and the ELSC (Bevis et al., 1995). In an updated version of the kinematic model, slower angular velocities of the Tonga volcanic arc were adopted and the diffuse plate boundary rejected based on the lack of evidence for tectonic activity (Figure 1, purple shaded region; Sleeper & Martinez, 2016, after Zellmer & Taylor, 2001). More recent kinematic reconstructions do not include the Niuafo'ou microplate (Lagemaat et al., 2018) as such, which is corroborated by a recent geological map of the Lau Basin (Stewart et al., 2022). Both studies do not acknowledge a diffuse plate boundary zone but state that spreading in the central Lau Basin mainly takes place at the CLSC and ELSC at the boundary between the Australian and Niuafo'ou-Tonga microplate (Figure 1, A-T orange shaded area), and that extension occurs locally and continues across the arc, just north of the "Volcano F" (Stewart et al., 2022).

Because of the presence of both well-defined and more distributed extensional domains, the Lau Basin is an ideal case study to investigate the processes at hand that lead to tectonic quiescence in systems that are in overall extension. A first analysis of the deep crustal structure of the Lau Basin was obtained along an 840-km long refraction seismic profile (Crawford et al., 2003). Their results revealed that in the diffuse plate boundary region the arc thickens from west to east and has an average crustal thickness of 7.5–8.5 km (Crawford et al., 2003). The study used a wide instrument-spacing at the seafloor with ∼42 km in between the deployed ocean-bottom seismometers (OBS), which limits the resolution of the resolved crustal structure. Here, we show results of seismic data acquired in the vicinity of the profile published by Crawford et al. (2003) in the central Lau Basin during the ARCHIMEDES-I expedition that took place in December 2018 and January 2019. The aim of our study is to resolve the crustal structure in the diffuse plate boundary region in more detail, with denser instrument spacing for a higher resolution (white line, Figure 1). We look for features that can explain tectonic quiescence in a system that is in overall extension. With this study, we complement and expand our understanding of the versatile tectonic activity in active back-arc systems.

2. Data and Methods

2.1. Data Acquisition

During the ARCHIMEDES-I expedition to the Lau Basin on the RV SONNE, 34 OBS were deployed along an E-W oriented seismic profile at 18°S (Figure 1). The 216 km long transect crosses the central Lau Basin from the CLSC in the west to the Tonga volcanic arc in the east. The OBS spacing was ∼6 km and simultaneously a 3.9 km long multi-channel seismic streamer was towed while shooting. The seismic source signal was generated with an air gun array consisting of 12 G-guns with a total volume of 84 L (5,440 cu.in.). The profile was shot at two different shot spacings in both directions, recorded on all OBS. Shots every 50 m served for the streamer and better resolution of the near offset arrivals on the OBS, while the 150 m shot spacing was chosen to reduce the noise in the water column from the previous shot to resolve the subsurface to larger depths. An airgun GPS was used for accurate shot locations. The OBS location on the seafloor was calculated from the direct water wave travel times. The OBS-stations were equipped with 4.5 Hz, three-component geophones and a HighTech Inc ULF/PCA hydrophone. The recorder's sampling rate was 250 Hz. The streamer consisted of 312 active channels, divided into hydrophone-group intervals of 12.5 m.

2.2. Data Processing

The data quality of all 34 OBS stations was good and offsets up to 75 km for five stations could be recovered (Figure 2 shows representative refraction seismic shot gathers and picked arrivals). The data were processed by applying a linear clock drift. Afterward, the continuous stream of data was cut into single shot traces. A predictive deconvolution of the signal was performed to compress the seismic wavelet to enhance the signal-noise ratio by attenuating the rining. The traces were then filtered time- and offset-dependent using bandpass filters with frequencies decreasing with larger offsets and times (8–30 Hz for offsets up to 12 km, 7–25 Hz for 12–20 km, 6–20 Hz for 20–50 km and 3–12 Hz for offsets >50 km). For the multichannel seismic (MCS) data, we applied a deconvolution to the raw data to remove the source signature from the seismic traces. Additional seismic processing steps included binning to common depth point (CDP, with intervals of 6.25 m), band-pass filtering (6–

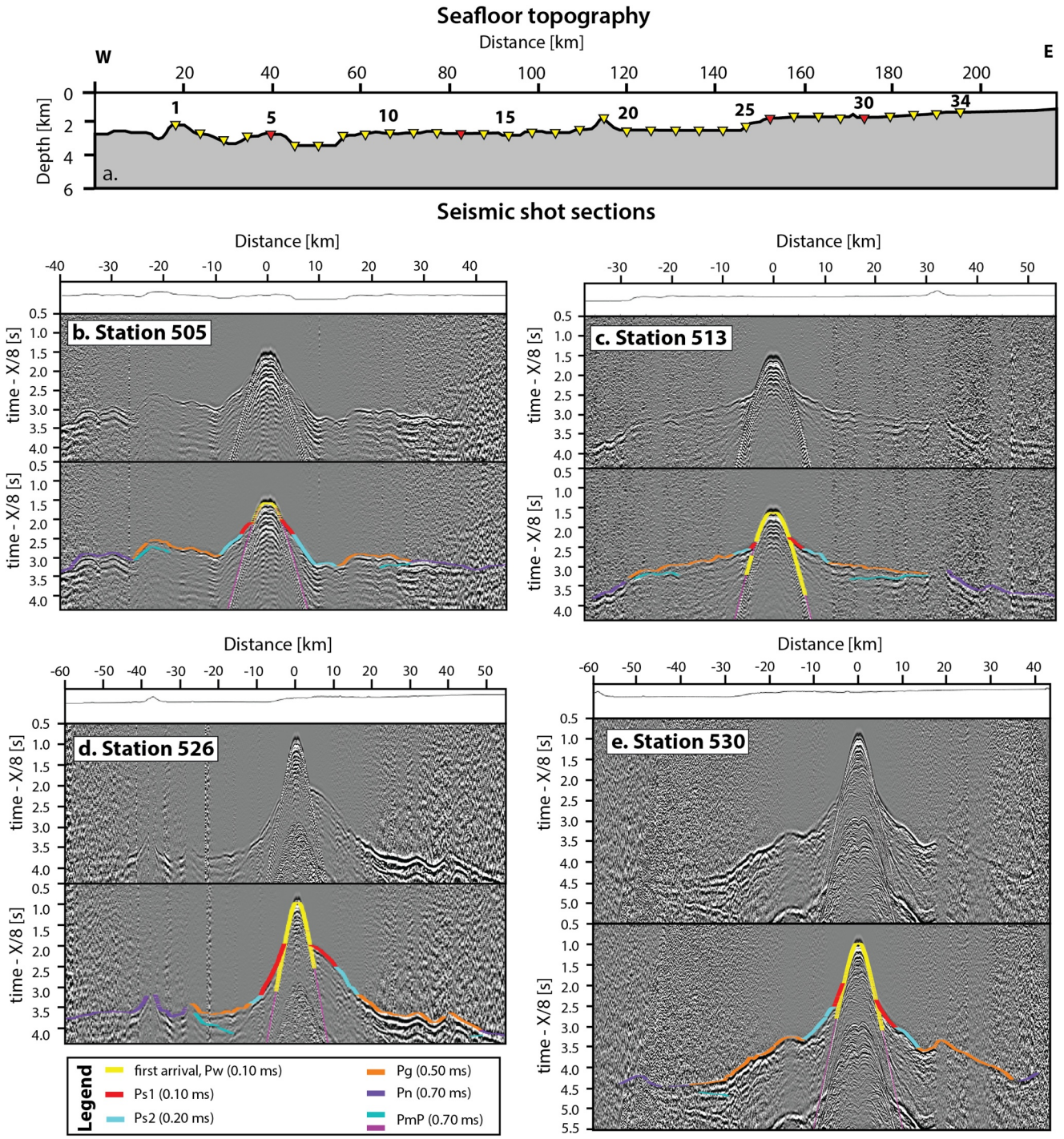

Figure 2. (a) Seafloor topography along profile BGR-205. Triangles indicate the location of the OBS. Panels (b–d) show refraction seismic data shot gathers (top) and picked phase arrivals (bottom) for stations (red triangles) toward the CLSC (505), in the back-arc region (516), at the transitional crust (526) and on the volcanic arc (530). The vertical extent of the picks shows the uncertainty.

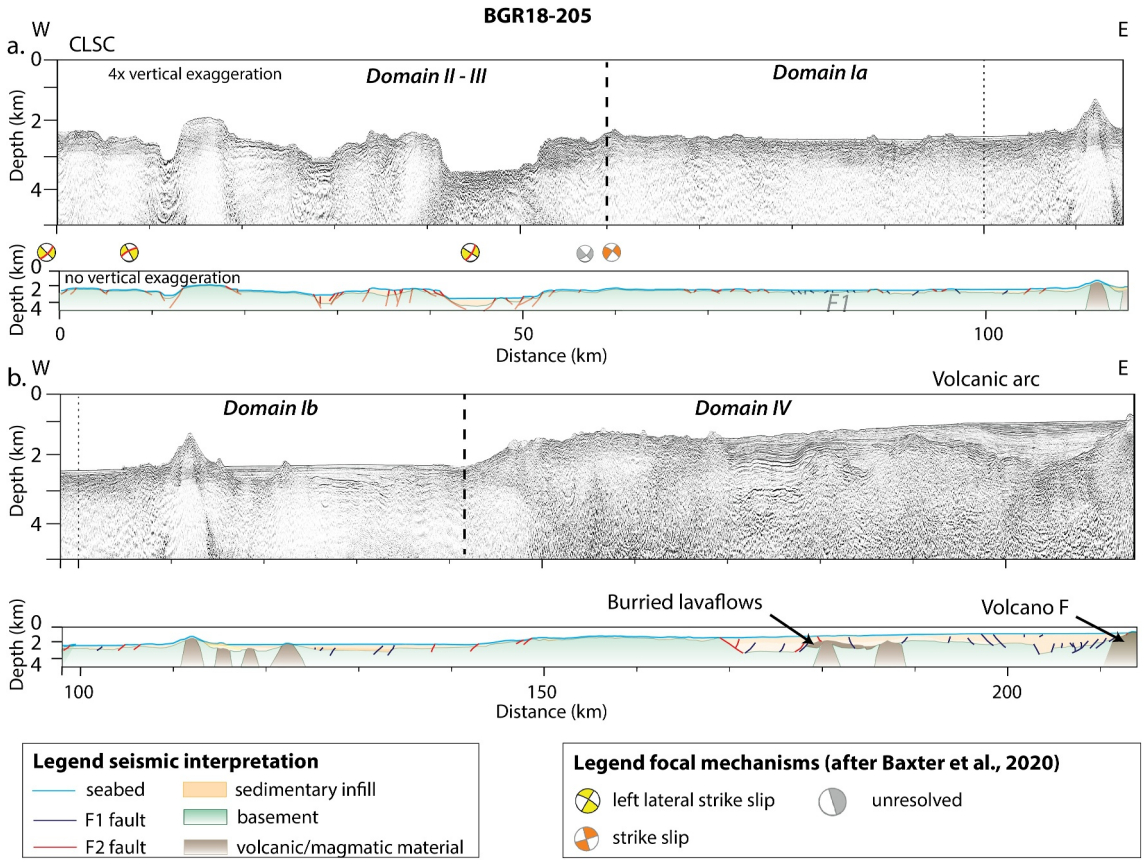

Figure 3. (a) 0–115 km of processed (top panel) and structurally interpreted (bottom panel) reflection seismic data. (b) and (a) 95–215 km of processed (top panel) and structurally interpreted reflection seismic data. The topography is rugged at the CLSC and in the back-arc domain (a), faults cross-cut the basement and are covered by sediments (F1 faults). Seamounts, volcanoes and buried lava flows and faults reaching the seafloor (F2 faults) are observed toward the east (b). Location of the "Volcano F" volcano after (Brandl et al., 2020).

80 Hz), true amplitude recovery, moveout-correction of CDP gathers, stacking and post-stack Kirchhoff time migration. The data was depth-converted prior to interpretation (Figure 3).

2.3. Traveltime Tomography

The primary and secondary phase arrivals were manually picked with the program *pasteup* (Fujie et al., 2008) that uses seismic unix (Stockwell, 1999) to display the segy-data. Steep-angle reflections from sediments are clear on the OBS that stand on sedimentary pockets and in the abyssal parts. The initial geometry of the acoustic basement was picked on the MCS data. The steep-angle sedimentary reflections were used in an initial forward model to estimate the P-wave velocity and thickness of the sediments. This is a crucial step for the traveltime tomographic inversion, where shallow regions of the model are poorly resolved. Since all rays travel through this area twice, errors would increase with depth without an accurate shallow P-wave velocity model. The crustal phase (*Pg*) is identified with pick uncertainties of 20 and 50 ms, for near and far offsets, respectively. The wide-angle reflection from the crust-mantle boundary (*PmP*) occurs between 25 and 35 km offset to the station and is observed at most stations. The refracted mantle arrival (*Pn*) is observed on most stations and it is visible up to 75 km offset from the station. On the western part of the profile, the *Pn* wave arrives at ~30 km. Closer to the arc the *Pn* wave arrives at ~40 km. A pick uncertainty of 70 ms was used for the *PmP* and *Pg* phases.

After picking, all refracted *Pg* (18,957 picks) and wide-angle reflected *PmP* (3,244 picks) traveltimes were jointly inverted in a Monte-Carlo approach using 100 different starting models with varying 1D P-wave velocity-depth models below the seafloor and sediments. Initial testing with a layer-stripping approach did not improve the results significantly. Besides varying the velocity and the velocity gradients with depth, the initial Moho reflector ranged between 14 and 18 km depth with 10 different versions varying in depth and shape. Afterward, an average

velocity model was calculated and served as input for the inversion of the mantle phases. The tomography software *tomo2D* (Korenaga et al., 2000) was used for the traveltime inversion. Due to the dense coverage of PmP-phases, our model has reliable values for the seismic velocity in the lower crust and for the crustal thickness. Local ray-bending was applied using smoothing (50 and 30 for velocity and depth) and damping (30 for both) constraints to regularize the iterative inversion. The regular grid cells were horizontally uniformly spaced with 350 m and vertically slightly increasing from 100 to 120 m with depth. To weigh the velocity and depth nodes equally, the weighting factor was set to $w = 1$ (Korenaga et al., 2000). A forward star with values of 10/15/1//8/0.0001 was chosen and five iterations were performed.

3. Results

3.1. P-Wave Tomography Results

The tomographic results along our profile (Figure 4a) show variations in the P-wave velocity distribution (Figure 4b). This profile overlaps with stations 15–24 (160–370 km) of the refraction seismic profile from Crawford et al. (2003, Figure 8). The standard deviation of our profile is generally below 0.2 and only increases toward the boundaries of the model, because of the decrease in ray-coverage and crossing rays toward the edges of the profile (Figures 4c and 4d).

Based on the lateral variations in P-wave velocity of the crust, we recognize four distinct domains (Figure 4b), of which three have been described in literature (Dunn & Martinez, 2011; Martinez & Taylor, 2002) and we have added a fourth Domain. Domain I corresponds to "older" crust that was already present before spreading started (Dunn & Martinez, 2011; Martinez & Taylor, 2002). Domain II-III consist of a relatively deep seafloor that has an abyssal hill tectonic fabric. This Domain features a relatively thin crust and is characterized by velocities of ∼5 km/s at 1 km into the crust (Dunn & Martinez, 2011; Martinez & Taylor, 2002). Domain IV represents thicker crust with seismic velocities typical for arc domains.

Sediments have an average P-wave velocity of 2.2–2.25 km/s in all domains. The first domain (Domain I) extends from 60 to 140 km and shows a relatively flat bathymetry. The upper crust in Domain I is characterized by a velocity gradient of ∼1 s^{-1}. We divide Domain I into two sub-domains: Ia extending from 60 to 100 km and Ib that stretches from 100 to 140 km. In our Domain Ib the P-wave velocities of the lower crust increase, whereas the P-wave velocities of the upper crust remain similar to those of Domain Ia. More specifically, between 115–135 km and 6–10 km below sea level (bsl), there is an increase in seismic velocity from 7.0 to 7.5 km/s in the lower crust. In the upper mantle of Domain Ib between 120 and 130 km, just below the Moho, seismic velocities reach 8.5 km/s. The crust has a ∼6–8 km thickness in Domain Ia and thickens to ∼7–9 km in Domain Ib.

Domains II and III (after Dunn & Martinez, 2011), between 15 and 60 km, host the CLSC and are characterized by a rugged seafloor (Figure 4a) with bathymetric depressions where the crustal thickness decreases to ∼5 km. Upper crust velocities in these domains increase from ∼3 to ∼6.4 km/s, top to bottom. These velocities are slightly higher than the 6.0 km/s upper crust velocities of Crawford et al. (2003). The lower crust has velocities between ∼6.4 and ∼7.2 km/s. The velocity gradient is ∼0.25 s^{-1}, comparable to Crawford et al. (2003). Our model shows a relatively flat and constant Moho depth of ∼9 km bsl in Domains Ia, II, and III, with mantle velocities of ∼8 km/s.

Domain IV extends from ∼140 km to the eastern profile end. The velocity gradient in the upper crust decreases (∼0.5 s^{-1}) compared to further west and the total crustal thickness increases from ∼9 km (at 140 km) to ∼13 km at 180 km profile distance below the volcanic arc. On our profile, the Moho depth increases gradually to ∼13 km with mantle velocities of ∼8 km/s. The lower crust shows a velocity gradient that is similar to the lower crust of Domain Ib of ∼0.25 s^{-1} and velocities that increase to ∼7.5 km/s above the seismic Moho. The 1.5 km thick, low velocity sediment package in Domain IV pinches out on the subsurface extent of the active "Volcano F" at the eastern end of the profile (Figure 4). At 115, 165, 185, 195, and 215 km high seismic velocities of 5 km/s locally reach to shallow depths approx. 1–1.5 km bsl, much shallower compared to the surroundings.

3.2. Seismic Reflection Results

The MCS data show structures down to 3 km bsl (Figure 3). The sediments are imaged as horizontally layered strata in basins along the profile and show very limited internal thickness variations. Especially in the deeper basins between 60 and 140 km, the package of sediments appears continuous with a general thickness of 500 m. We observe similar domains as the ones identified on the OBS traveltime tomography. The surface expression of

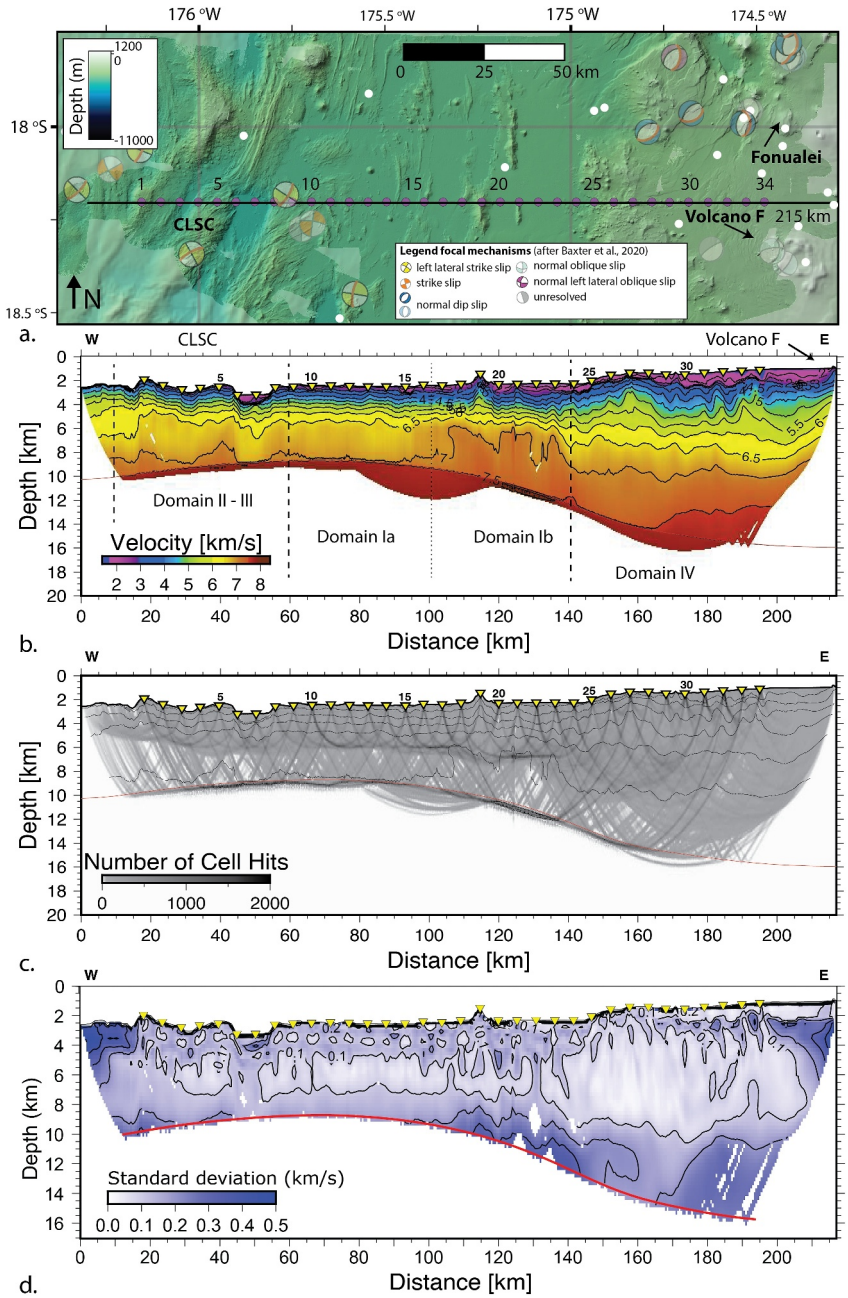

Figure 4. (a) Detailed high-resolution bathymetry along profile BGR-205 acquired during the ARCHIMEDES-I expedition (Hannington et al., 2019), overlaying bathymetry retrieved from the open access GEBCO bathymetric database. White dots indicate the locations of shallow earthquakes (<10 km depth) that have been recorded since 1964, retrieved from the IRIS database (Trabant et al., 2012). (b) Average velocity model of the crustal structure along profile BGR-205. Based on changes in the velocity gradient and absolute velocities, the profile is divided into four domains. (c) Derivative weight sum for the individual nodes of the model grid, representing the ray coverage. (d) The standard deviation is between 0 and 0.2 for crustal levels until 9 km. Below 9 km the standard deviation of the models increases to 0.2–0.3. Locations "Fonualei" and "Volcano F" volcanoes after Brandl et al. (2020).

Domain II-III consists of steeply dipping normal faults and a rough seafloor topography at the CLSC (Figure 3a, 0–60 km) and shallow basins with limited infill that cover faults in the basement of Domain Ia (F1 faults, Figure 3, 60–100 km). Active growth structures and syn-tectonic features are absent in the shallower parts of the sedimentary infill. In Domain Ib between 100 and 140 km, elongated features pierce through the sediment pile while the sediment package thickens toward the volcanic arc. Domain IV covers the volcanic arc of this profile where

the bathymetry is shallower and a thick sediment package covers volcanic features at 2 and 3 km bsl (Figure 3b, between 140 and 210 km). On the volcanic arc, between 170 and 210 km, the sediment thickness is ∼1.5 km. At 205–210 km the sedimentary pile completely disappears, while onlapping on a structure with an isotropic seismic character, which is attributed to the subsurface extension of "Volcano F." The internal structure of the sedimentary layers on the volcanic arc appears more varied than in the shallow basins at the western profile half. Some brighter, seismic isotropic bodies varying in thickness and size are observed piercing through the sedimentary pile (e.g., at 115, 165, and 215 km). Between 2 and 3 km depth, between 180 and 190 km, conical isotropic bodies with onlapping bright reflectors pierce through the oldest sediments but are covered by a younger sedimentary pile.

4. Discussion

4.1. Crustal Structure

From the average P-wave velocity model, we have identified that the crustal thickness changes from ∼6 to 8 km in the back-arc region (Domains I-III) to ∼13 km below the volcanic arc (Domain IV). For Domains I-III, the crustal thickness is generally 2 and 3 km thinner than the crustal thickness of this region on the profile of Crawford et al. (2003). The general seismic velocity distribution and gradients in Domains I-III are comparable to common back-arc basin crust (Arai & Dunn, 2014; Grevemeyer et al., 2021). The difference in the velocity of the lower crust toward the west and east of 45 km profile length might represent the boundary between young crust formed at the CLSC and older crust of the ELSC (Crawford et al., 2003). The MCS data in Domains I-III show clearly imaged sediments filling in the basins from 2 Ma until today, following the magnetic chrons of Taylor et al. (1996). The sediments cover older fault structures and onlap on apparent seamounts, which is indicative for previous extension and current tectonic quiescence (Figure 3b).

The change in the P-wave velocity structure that occurs in the transition from back-arc to arc crust (100–140 km, Domain Ib, Figure 4b) is much more subtle than the dramatic crustal thinning that was modeled and interpreted by Crawford et al. (2003). At 300–320 km along their profile, which compares to 105–125 km along our profile in Domain Ib, their crust suddenly thins to 4–4.5 km. The Moho depth of our model shows the opposite and gradually thickens eastwards to ∼13 km. Isotropic bodies on the MCS data between 110 and 145 km are interpreted as buried volcanoes, that are rooted in high velocity lower crust (7.0–7.5 km/s). This area represents the margin of the volcanic arc (Figures 3 and 4). A higher P-wave velocity in the lower crust at the margin of the volcanic arc may originate from hydrous melting (Arai & Dunn, 2014) or from invading mantle material (Grevemeyer et al., 2021).

The general velocity gradient of ∼0.5 s^{-1} in the upper crust of Domain IV, the seismic P-wave velocities of 6.5–7.5 km/s in the lower crust and the 13 km thick crust are comparable to standard arc-crust which consists predominantly of mafic material (Calvert, 2011). The increased velocities in the upper crust at 165, 185, and 195 km that correspond to vertical isotropic bodies at 2 and 3 km depth imaged on the MCS data are interpreted as remnant volcanoes. Horizontal, thinner bodies are interpreted as lava flows. The crustal velocities of these volcanoes are not as high as in Domain Ib, and we hypothesize that these volcanoes are younger because they are located closer to the volcanic arc. This interpretation is supported by the location of the active "Volcano F" (Brandl et al., 2020), on the eastern end of our profile. A drill-core into the sediments of Domains I and IV to the basement and/or the top of one of the volcanic structures in Domain Ib and IV would provide better time constraints about the onset of volcanism and their activity through time.

4.2. Tectonic Activity in the Back-Arc Domain

The interpretation of the reflection and refraction seismic data allowed us to investigate the previously observed seismically active and inactive zones in the Lau Basin (Baxter et al., 2020) within an overall extending system. At the CLSC, between 15 and 60 km in Domain II-III, we observe rugged topography (Figure 5) that coincides with steeply dipping NW-SE running normal faults on the MCS data (Figure 3) that actively offset the seafloor. The crust is only 5 km thick, comparable to the crust further north along the FRSC (Jegen et al., 2023; Schmid et al., 2020), which is relatively thin compared to the general 6–8 km thickness in Domains I-III. The observations confirm active thinning and extension accommodation at the CLSC, which is also recognized with magnetic anomalies (Taylor et al., 1996; Zellmer & Taylor, 2001). The style of extension in this particular region has been interpreted as bookshelf faulting, which is the result of southward propagating rifts, leading to abandoned branches of the ELSC and tectonic activity at the CLSC (Wetzel et al., 1993).

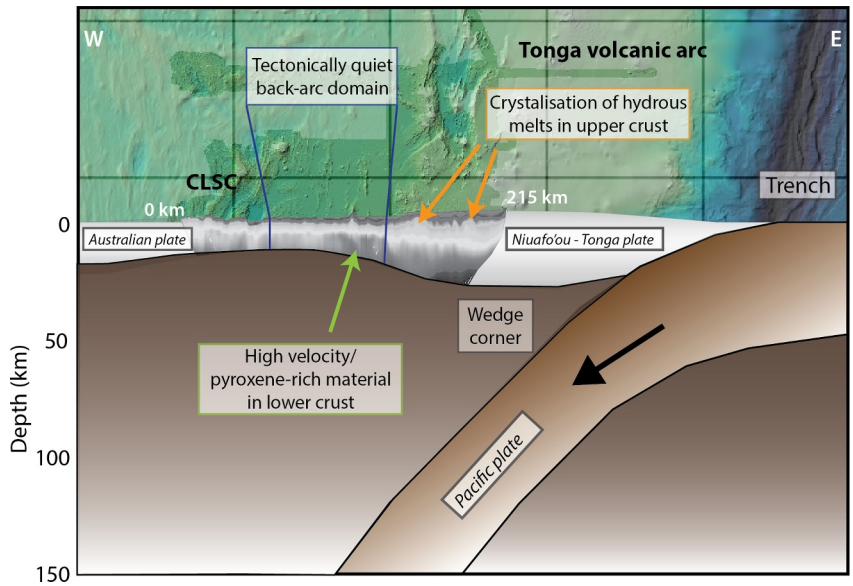

Figure 5. Cartoon showing the tectonically quiet zone (60–140 km) in between the volcanic arc and the CLSC. Pyroxene-rich mantle can occur at depth below volcanoes, which will result in high-velocity bodies at lower crustal levels. Crystalisation of hydrous melts above the mantle wedge lead to high velocity bodies at upper crustal levels.

The seismically inactive (Baxter et al., 2020) part of our Domain I (60–140 km, Figure 5), consists of the most homogeneous crustal structure, where the MCS data show a lack of growth faults and syn-tectonic structures and the presence of undisturbed sediments (Figure 3). These observations in combination with the absence of seismicity confirm the current tectonic quiescence in this region (Figure 5). This is in contrast with the crustal structure investigated further north along the western margin of the Tonga volcanic arc (Schmid et al., 2020). At 17° 20′S, the crustal structure is heterogeneous, with domains that resemble oceanic crust and domains that resemble arc crust or a more "hydrous" crust that has been augmented by slab-derived fluids. Even further north, at 16°S, the geochemistry of the crust is strongly influenced by the subduction. There, the crust has been overprinted by a tectonic component as observed in the seismic data implying tectonic activity (Jegen et al., 2023). Despite the current seismic inactivity, we do not exclude that extension was accommodated in these seismic inactive regions in the past. The buried faults (F1 faults, Figure 3) with similarly thick sediment packages actually indicate former rifting, which can be interpreted as early/extinct branches of the propagating rift (Wetzel et al., 1993).

In our area, we thus find evidence for current tectonic activity at the CLSC (Figure 1, yellow shaded area), which has been reported by other studies (Baxter et al., 2020; Martinez & Taylor, 2002; Stewart et al., 2022), but not closer to the arc, even though at the southern tip of the FRSC (Stewart et al., 2022), in between the volcanoes "Fonualei" and "Volcano F" (Figure 4a) tectonic activity has been reported. Unfortunately this region is not covered by our profile. The sediment infill of the basins flanked by F2-faults between 60 km and 100 is continuous without thickness changes, indicating that these faults have been inactive for some time. They may have been active in the past, causing depocenters to form that have not completely filled up yet. On our high-resolution refraction and reflection seismic data we thus do not find evidence for current tectonic activity between 60 and 140 km along our profile in between the CLSC and the Tonga volcanic arc. This has also been proposed by Sleeper and Martinez (2016) after studying global earthquake catalogs (Trabant et al., 2012) and was shown by Conder and Wiens (2011). We therefore suggest that the Niuafo'ou-Tonga microplate could be regarded as a larger plate with local zones of intraplate deformation.

4.3. Volcanic Activity Along Our Profile

The high P-wave velocities in the upper crust in Domain Ib correspond to volcanic remnants on our MCS data. High P-wave velocities in the upper crust can be produced by the crystalisation of hydrous melts (Arai & Dunn, 2014; Eason & Dunn, 2015). On our profile, the volcanic remnants are covered by sediments, which

indicates that they became extinct and are now inactive. They are interpreted here as the oldest volcanic material and the oldest expressions of the volcanic arc along our profile, but no age-dating on these buried volcanoes exists. We assume that, during their extinction, the magma chamber cooled down and solidified. To reach the high lower crustal and mantle velocities around 115 km profile distance, the intrusive, cooled down material, might have a higher pyroxene content (7.2 km/s; Carlson & Miller, 2004) or it may consist of pyroxenite (7.8 km/s; Christensen, 1978). The presence of pyroxenite in the lower crust might be supported by elevated velocities (8.5 km/s) in the uppermost mantle (between 120 and 140 km at 11 km dbls). These occurrences potentially originate from remnant magmatic material with high pyroxene and/or olivine content that still resides at depth, which fits with the general understanding that most occurrences of mantle pyroxenite are thought to have formed in the supra-subduction setting (Belousov et al., 2021). An example is the ophiolite of Cyprus in which intrusive material with a high pyroxene and olivine content has been reported (Benn & Laurent, 1987). This ophiolite is considered to have formed in a supra-subduction tectonic setting (Muenow et al., 1980), probably close to the wedge corner (Pearce & Robinson, 2010).

The older volcanoes go extinct and solidify while the slab retreats further. The volcanic arc will migrate with the retreating the slab in the direction of the trench. This migration with the retreating slab of the volcanic arcs has been observed elsewhere as well. In the Scotia Sea for example, the Ancestral South Sandwich Arc (Pearce et al., 2014) is considered a pre-cursor of the current South Sandwich volcanic arc. When slab roll-back continued, the arc migrated with the trench, leaving the Ancestral South Sandwich Arc and an eventual seismically inactive West and Central Scotia behind, starting a new spreading center at the East Scotia Ridge.

5. Conclusions

We investigated a seismically inactive zone in an overall extending back-arc system at 18°S, the Lau Basin (southwest Pacific Ocean) using a high resolution P-wave velocity model and multi-channel seismic data. We identified a gradual increase in crustal thickness from 6 to 8 km in the back-arc domain (Domains I-III) and approximately 13 km below the arc (Domain IV). Lower crustal velocities increase to 7.5 km/s toward the volcanic arc, marking the change from back-arc to arc crust (Domain Ib). In this domain, we identified remnant volcanic material in the back-arc–arc transition. Extension is currently accommodated at the CLSC, but earlier, now inactive, extensional structures are observed in between the CLSC and the Tonga volcanic arc. We do not find evidence for an active plate boundary in the central Lau Basin between 60 and 140 km along our profile and interpret this part as a tectonically quiet region within an overall extending back-arc domain. We relate the high P-wave velocities that we observe in the upper crust to the crystalisation of hydrous melts, whereas the high P-wave velocities in the lower crust could be the result of the crystalisation of pyroxene-rich material.

Appendix A: SO267 Science Party Members and Affiliations

N. Augustin[1], U. Barckhausen[2], P. Brandl[1], C. Devey[1], M. Engels[2], M. Hannington[1,3] (Chief Scientist of SO267), I. Heyde[2], A. Jegen[1], I. Klaucke[1], F. Petersen[1,4], S. Petersen[1], M. Riedel[1], F. Schmid[1,5], B. Schramm[1,2], M. Stewart[6], M. Weber[7], R. Werner[1,†]

[1]GEOMAR, Helmholtz Center for Ocean Research Kiel, Kiel, Germany

[2]BGR, Federal Institute for Geosciences and Natural Resources, Hannover, Germany

[3]Department of Earth and Environmental Sciences, Mount Royal University, Calgary, Canada

[4]Center for Ocean and Society, Kiel, Schleswig-Holstein, DE

[5]K.U.M. Umwelt- und Meerestechnik Kiel GmbH, Kiel, Germany

[6]Department of Earth and Environmental Sciences, University of Ottawa, Ontario, Canada

[7]GFZ, German Research Center for Geosciences, Potsdam, Germany

[†]Deceased 1 August 2022

Data Availability Statement

The refraction seismic data (Kopp et al., 2023) and the reflection seismic data (Schnabel et al., 2023) are publicly available and can be accessed via the PANGAEA.

Acknowledgments
AB conducted this work under the Alexander von Humboldt Postdoctoral Fellowship and thanks the AvH Foundation for their support. The captain and crew of "RV Sonne" as well as the scientific party of the SO267 "ARCHIMEDES-I" expedition are thanked for their physical and mental contribution and support. We thank Fernando Martinez, Camilla Palmiotto, and an anonymous reviewer for the constructive feedback during the review process, which greatly improved our manuscript. Cruise SO267 and data acquisition were funded by the "Bundesministerium für Bildung und Forschung" (BMBF) Grants 03G0267A and 03G0267B with additional financial and logistical support and use of large-scale equipment from GEOMAR and BGR.

References

Anderson, M. O., Norris-Julseth, C., Rubin, K. H., Haase, K., Hannington, M. D., Baxter, A. T., & Stewart, M. S. (2021). Geologic and structural evolution of the NE Lau Basin, Tonga: Morphotectonic analysis and classification of structures using shallow seismicity. *Frontiers in Earth Science*, *9*, 1–24. https://doi.org/10.3389/feart.2021.665185

Arai, R., & Dunn, R. A. (2014). Seismological study of Lau back arc crust: Mantle water, magmatic differentiation, and a compositionally zoned basin. *Earth and Planetary Science Letters*, *390*, 304–317. https://doi.org/10.1016/j.epsl.2014.01.014

Artemieva, I. M. (2023). Back-arc basins: A global view from geophysical synthesis and analysis. *Earth-Science Reviews*, *236*, 104242. https://doi.org/10.1016/j.earscirev.2022.104242

Baxter, A. T., Hannington, M. D., Stewart, M. S., Emberley, J. M., Breker, K., Krätschell, A., et al. (2020). Shallow seismicity and the classification of structures in the Lau Back-Arc basin. *Geochemistry, Geophysics, Geosystems*, *21*(7), e2020GC008924. https://doi.org/10.1029/2020GC008924

Belousov, I., Batanova, V., Sobolev, A., Savelieva, G., Danyushevsky, L., & Draayers, E. (2021). Lithos Pyroxenites from mantle section of Voykar Ophiolite—Melt/peridotite reaction and crystallization in SSZ mantle. *Lithos*, *388–389*, 106063. https://doi.org/10.1016/j.lithos.2021.106063

Beniest, A., Brun, J. P., Gorini, C., Crombez, V., Deschamps, R., Hamon, Y., & Smit, J. (2016). Interaction between trench retreat and Anatolian escape as recorded by neogene basins in the northern Aegean Sea. *Marine and Petroleum Geology*, *77*, 30–42. https://doi.org/10.1016/j.marpetgeo.2016.05.011

Benn, K., & Laurent, R. (1987). Intrusive suite documented in the Troodos ophiolite plutonic complex, Cyprus. *Geology*, *15*(9), 821–824. https://doi.org/10.1130/0091-7613(1987)15%3C821:ISDITT%3E2.0.CO;2

Bevis, M., Taylor, F. W., Schutz, B. E., Recy, J., Isacks, B. L., Helu, S., et al. (1995). Geodetic observations of very rapid convergence and back-arc extension at the Tonga arc. *Nature*, *374*(6519), 249–251. https://doi.org/10.1038/374249a0

Brandl, P. A., Schmid, F., Augustin, N., Grevemeyer, I., Arculus, R. J., Devey, C. W., et al. (2020). The 6–8 Aug 2019 eruption of "Volcano F" in the Tofua Arc, Tonga. *Journal of Volcanology and Geothermal Research*, *390*, 106695. https://doi.org/10.1016/j.jvolgeores.2019.106695

Brun, J.-P., Faccenna, C., Gueydan, F., Sokoutis, D., Philippon, M., Kydonakis, K., & Gorini, C. (2016). The two-stage Aegean extension, from localized to distributed, a result of slab rollback acceleration. *Canadian Journal of Earth Sciences*, *53*(11), 1142–1157. https://doi.org/10.1139/cjes-2015-0203

Calvert, A. J. (2011). The seismic structure of Island arc crust. In D. Brown & P. D. Ryan (Eds.), *Arc-continental collission* (pp. 87–119). Frontiers in Earth Sciences. https://doi.org/10.1007/978-3-540-88558-0

Carlson, R. L., & Miller, D. J. (2004). Influence of pressure and mineralogy on seismic velocities in oceanic gabbros: Implications for the composition and state of the lower oceanic crust. *Journal of Geophysical Research*, *109*(B09205), 1–17. https://doi.org/10.1029/2003JB002699

Chase, C. G. (1971). Tectonic history of the Fiji plateau. *Bulletin of the Geological Society of America*, *82*(11), 3087–3110. https://doi.org/10.1130/0016-7606(1971)82[3087:THOTFP]2.0.CO;2

Christensen, I. (1978). Ophiolites, seismic velocities and oceanic crustal structure. *Tectonophysics*, *47*(1–2), 131–157. https://doi.org/10.1016/0040-1951(78)90155-5

Conder, J. A., & Wiens, D. A. (2011). Shallow seismicity and tectonics of the central and northern Lau Basin. *Earth and Planetary Science Letters*, *304*(3–4), 538–546. https://doi.org/10.1016/j.epsl.2011.02.032

Crawford, W. C., Hildebrand, J. A., Dorman, L. M., Webb, S. C., & Wiens, D. A. (2003). Tonga Ridge and Lau Basin crustal structure from seismic refraction data. *Journal of Geophysical Research*, *108*(B4), 2195. https://doi.org/10.1029/2001jb001435

Dunn, R. A., & Martinez, F. (2011). Contrasting crustal production and rapid mantle transitions beneath back-arc ridges. *Nature*, *469*(7329), 198–202. https://doi.org/10.1038/nature09690

Eagles, G., Livermore, R. A., Fairhead, J. D., & Morris, P. (2005). Tectonic evolution of the west Scotia Sea. *Journal of Geophysical Research*, *110*(2), 1–19. https://doi.org/10.1029/2004JB003154

Eason, D. E., & Dunn, R. A. (2015). Petrogenesis and structure of oceanic crust in the Lau back-arc basin. *Earth and Planetary Science Letters*, *429*, 128–138. https://doi.org/10.1016/j.epsl.2015.07.065

Fujie, G., Kasahara, J., Murase, K., Mochizuki, K., & Kaneda, Y. (2008). Interactive analysis tools for the wide-angle seismic data for crustal structure study (Technical Report). *Exploration Geophysics*, *39*(1), 26–33. https://doi.org/10.1071/EG08006

Grevemeyer, I., Kodaira, S., Fujie, G., & Takahashi, N. (2021). Structure of oceanic crust in back-arc basins modulated by mantle source heterogeneity. *Geology*, *49*(4), 468–472. https://doi.org/10.1130/G48407.1

Hannington, M. D., Kopp, H., & Schnabel, M. (2019). RV Sonne cruise report SO267—ARCHIMEDES 1: Arc rifting, metallogeny and microplate evolution—An integrated geodynamic, magmatic and hydrothermal study of the Fonualei Rift system, NE Lau Basin. *GEOMAR-Report*, *49*(49). https://doi.org/10.3289/GEOMAR_REP_NS_49_2019

Jegen, A., Dannowski, A., Schnabel, M., Barckhausen, U., Brandl, P. A., Riedel, M., et al. (2023). Extension dynamics of the northern Fonualei Rift and spreading center and the southern Mangatolu Triple Junction in the Lau Basin at 16°S. *Geochemistry, Geophysics, Geosystems*, *24*(4), 1–23. https://doi.org/10.1029/2022GC010550

Karig, D. E. (1970). Ridges and basins of the Tonga-Kermadec Island arc system. *Journal of Geophysical Research*, *75*(2), 239–254. https://doi.org/10.1029/JB075i002p00239

Kopp, H., Beniest, A., & Dannowski, A. (2023). Seismic refraction and wide-angle reflection OBS data from profile P05 during SONNE cruise SO267 (ARCHIMEDES), Lau Basin [Dataset]. *Pangea*. https://doi.org/10.1594/PANGAEA.959000

Korenaga, J., Holbrook, W. S., Kent, G. M., Kelemen, P. B., Detrick, R. S., Larsen, H., et al. (2000). Crustal structure of the southeast Greenland margin from joint refraction and reflection seismic tomography. *Journal of Geophysical Research*, *105*(B9), 21591–21614. https://doi.org/10.1029/2000JB900188

Van De Lagemaat, S. H. A., Van Hinsbergen, D. J. J., Boschman, L. M., Kamp, P. J. J., & Spakman, W. (2018). Southwest Pacific absolute alate kinematic reconstruction reveals major Cenozoic Tonga-Kermadec slab dragging. *Tectonics*, *37*(8), 2647–2674. https://doi.org/10.1029/2017TC004901

Makris, J., Papoulia, J., Papanikolaou, D., & Fasoulaka, C. (2022). Tectonophysics crustal structure beneath the cyclades metamorphic core complex, aegean. *Tectonophysics*, *842*, 229585. https://doi.org/10.1016/j.tecto.2022.229585

Martinez, F., & Taylor, B. (2002). Mantle wedge control on back-arc crustal accretion. *Nature*, *416*(6879), 417–420. https://doi.org/10.1038/416417a

Muenow, D. W., Liu, N. W. K., Garcia, M. O., & Saunders, A. D. (1980). Volatiles in submarine volcanic rocks from the spreading axis of the East Scotia Sea back-arc basin. *Earth and Planetary Science Letters*, *47*(2), 272–278. https://doi.org/10.1016/0012-821X(80)90043-6

Palmiotto, C., Ficini, E., Loreto, M. F., Muccini, F., & Cuffaro, M. (2022). Back-Arc spreading centers and superfast subduction: The case of the northern Lau Basin (SW Pacific Ocean). *Goesciences*, *12*(50), 1–17. https://doi.org/10.3390/geosciences12020050

Pearce, J. A., Hastie, A. R., Leat, P. T., Dalziel, I. W., Lawver, L. A., Barker, P. F., et al. (2014). Composition and evolution of the Ancestral South Sandwich arc: Implications for the flow of deep ocean water and mantle through the drake passage gateway. *Global and Planetary Change*, *123*, 298–322. https://doi.org/10.1016/j.gloplacha.2014.08.017

Pearce, J. A., & Robinson, P. T. (2010). The Troodos ophiolitic complex probably formed in a subduction initiation, slab edge setting. *Gondwana Research*, *18*(1), 60–81. https://doi.org/10.1016/j.gr.2009.12.003

Ruellan, E., Delteil, J., Wright, I., & Matsumoto, T. (2003). From rifting to active spreading in the Lau Basin-Havre trough backarc system (SW Pacific): Locking/unlocking induced by seamount chain subduction. *Geochemistry, Geophysics, Geosystems*, *4*(5). https://doi.org/10.1029/2001GC000261

Schellart, W. P., Strak, V., Beniest, A., Duarte, J. C., & Rosas, F. M. (2023). Subduction invasion polarity switch from the Pacific to the Atlantic Ocean: A new geodynamic model of subduction initiation based on the Scotia Sea region. *Earth-Science Reviews*, *236*, 104277. https://doi.org/10.1016/j.earscirev.2022.104277

Schmid, F., Kopp, H., Schnabel, M., Dannowski, A., Heyde, I., Riedel, M., et al. (2020). Crustal structure of the Niuafo'ou Microplate and Fonualei Rift and Spreading Center in the northeastern Lau Basin, Southwestern Pacific. *Journal of Geophysical Research: Solid Earth*, *125*(6), 1–21. https://doi.org/10.1029/2019JB019184

Schnabel, M., Beniest, A., & Kopp, H. (2023). Seismic reflection processed data of profile P05 (BGR18-205) during SONNE cruise SO267, Lau Basin, South Pacific Ocean [Dataset]. *Pangea*. https://doi.org/10.1594/PANGAEA.960348

Sdrolias, M., & Müller, R. D. (2006). Controls on back-arc basin formation. *Geochemistry, Geophysics, Geosystems*, *7*(Q04016), 1–40. https://doi.org/10.1029/2005GC001090

Sleeper, J. D., & Martinez, F. (2016). Geology and kinematics of the Niuafo'ou microplate in the northern Lau Basin. *Journal of Geophysical Research: Solid Earth*, *121*(7), 4852–4875. https://doi.org/10.1002/2016JB013051

Smith, I. E. M., & Price, R. C. (2006). The Tonga—Kermadec arc and Havre—Lau back-arc system: Their role in the development of tectonic and magmatic models for the western Pacific. *Journal of Volcanology and Geothermal Research*, *156*(3–4), 315–331. https://doi.org/10.1016/j.jvolgeores.2006.03.006

Stewart, M., Hannington, M., Emberley, J., Baxter, A. T., Krätschell, A., Petersen, S., et al. (2022). A new geological map of the Lau Basin (southwestern Pacific Ocean) reveals crustal growth processes in arc-backarc systems. *Geosphere*, *18*(2), 910–943. https://doi.org/10.1130/GES02340.1

Stockwell, J. W. J. (1999). The CWP/SU: Seismic Un*x package. *Computers & Geosciences*, *25*(4), 415–419. https://doi.org/10.1016/S0098-3004(98)00145-9

Taylor, B., Zellmer, K., Martinez, F., & Goodliffe, A. (1996). Sea-floor spreading in the Lau back-arc basin. *Earth and Planetary Science Letters*, *144*(1–2), 35–40. https://doi.org/10.1016/0012-821X(96)00148-3

Tirel, C., Gueydan, F., Tiberi, C., & Brun, J. P. (2004). Aegean crustal thickness inferred from gravity inversion. Geodynamical implications. *Earth and Planetary Science Letters*, *228*(228), 267–280. https://doi.org/10.1016/j.epsl.2004.10.023

Trabant, C., Hutko, A. R., Bahavar, M., Karstens, R., Ahern, T., & Aster, R. (2012). Data products at the IRIS DMC: Stepping stones for research and other applications. *Seismological Research Letters*, *83*(5), 846–854. https://doi.org/10.1785/0220120032

Wetzel, L. R., Wiens, D. A., & Kleinrock, M. C. (1993). Evidence from earthquakes for bookshelf faulting at large non-transform ridge offsets. *Nature*, *362*(6417), 235–237. https://doi.org/10.1038/362235a0

Zellmer, K. E., & Taylor, B. (2001). A three-plate kinematic model for Lau Basin opening. *Geochemistry, Geophysics, Geosystems*, *2*(5), 1525–2027. https://doi.org/10.1029/2000GC000106